Article

Theoretical Analysis of Experimental Data of Sodium Diffusion in Oxidized Molybdenum Thin Films

Orlando Ayala [1,2,*], **Benjamin Belfore** [2], **Tasnuva Ashrafee** [2], **John Akwari** [2], **Grace Rajan** [2], **Shankar Karki** [2], **Deewakar Poudel** [2] **and Sylvain Marsillac** [2]

1   Department of Engineering Technology, Old Dominion University, Norfolk, VA 23529, USA
2   Virginia Institute of Photovoltaics, Old Dominion University, Norfolk, VA 23529, USA;
    bbelf001@odu.edu (B.B.); tashr001@odu.edu (T.A.); cakwa001@odu.edu (J.A.); gcher002@odu.edu (G.R.);
    skark002@odu.edu (S.K.); dpoud001@odu.edu (D.P.); smarsill@odu.edu (S.M.)
*   Correspondence: oayala@odu.edu

Abstract: In this work, the diffusion process of sodium (Na) in molybdenum (Mo) thin films while it was deposited on soda lime glass (SLG) was studied. A small amount of oxygen was present in the chamber while the direct-current (DC) magnetron sputtering was used for the deposition. The substrate temperatures were varied to observe its effect. Such molybdenum films, with or without oxidations, are often used in thin film solar cells, either as back contact or as hole transport layers. Secondary ion mass spectrometry (SIMS) was used to quantify the concentration of the species. A grain diffusion mechanistic model incorporating the effect of grain and grain boundary geometrical shape and size was developed. The model was used to provide an in-depth theoretical analysis of the sodium diffusion in molybdenum thin films that lead to the measured SIMS data. It was observed that not only diffusion coefficients should be considered when analyzing diffusion processes in thin films but also the ratio of grain boundary size to grain size. Both depend on substrate temperature and directly affect the amount of diffused species in the film. The data were analyzed under the light of the film growth speed versus diffusion front speed, the effect of oxygen content, and the effect of substrate temperature on the overall diffusion process. The temperature inversely affects the ratio of grain boundary size and grain size and directly affects the diffusion coefficient, which leads to a preferable temperature at which the highest amount of alkali can be found in the film.

Keywords: modeling; thin films; diffusion; molybdenum

1. Introduction

High efficiency Cu(In,Ga)Se$_2$ (CIGS) solar cells are always achieved by incorporating small amount of sodium (Na) into the CIGS film to improve open-circuit voltage and fill factor [1]. molybdenum (Mo) coated soda-lime glass (SLG) is a common substrate used for CIGS solar cells. SLG acts as a source of Na and the Mo thin film serves as transport gate for Na diffusion from the SLG into the CIGS. On the other hand, Chirila et al. [2] found that a Potassium (K) post-deposition treatment on CIGS was beneficial for its performance but, interestingly, found a depletion of Na as a result of increased K concentration. The authors argued that the exchange occurred due to an ion exchange reaction. It is, therefore, particularly important to study and understand the diffusivity of Na and K in Mo thin films and the diffusion mechanism that occurs. To this date and to the best of our knowledge, very few studies have been reported on directly characterizing the diffusion and/or providing diffusivity constants in Mo thin films [3]. And on top of that, none of them have considered directly the grain size effect on the SIMS intensity data, which, as it will be shown later, it likely biases the measured diffusion coefficient.

Another key element to take into account for the study of alkali diffusion in Mo is oxygen. Oxygen has effectively been found to facilitate sodium diffusion through Mo and CIGS films [3–8] and has been used to ensure higher adhesion on flexible substrates [9].

Using X-ray photoelectron spectroscopy (XPS) and secondary ion mass spectrometry (SIMS), researchers found oxygen content up to 30 at.% O in the films and up to 53 at.% O on the surface. Some authors noted an increased in oxygen presence with an increase of film "porosity" and hypothesized that some of the oxygen came from the Na_2O present in the glass [8,10]. Other researchers have purposely added oxygen to the films for a more systematic study of its effect on sodium diffusion. Zellner et al. annealed samples of SLG/Mo/CIGS in an environment of 1.33 mPa (10^{-5} Torr) of oxygen to force its presence in the film [11]. Similarly, Yoon et al. [6] oxidized SLG/Mo/CIGS sample by annealing at 200 °C under ambient O_2 gas. On the other hand, Forest et al. [3] added oxygen to Mo film surface by heating the piece in ambient air at 200 °C. They had a range of oxygen content on the Mo film surface from 16 at.% to 65 at.%. In all those cases, the films were already fabricated.

In this study, a constant amount of oxygen was introduced into the chamber during sputtering to ensure a more uniform oxygen content throughout the film. In contrast to the previous work on sodium diffusion in molybdenum thin films, in this work, the sodium diffusion occurs while Mo films are deposited on soda lime glass. We propose a theoretical mechanistic model and use it to provide an in-depth theoretical analysis of the sodium diffusion in molybdenum thin films that lead to the registered SIMS data. Furthermore, the effect of grain and grain boundary sizes on the SIMS data, typically used to study concentration profiles of species after a diffusion process, was investigated.

The paper is organized as follows. In Section 2, the experimental details for fabrication of the molybdenum thin films are presented. Characterization techniques and the respective results are also discussed. Section 3 lays out a theoretical mechanistic modeling background needed to better understand and model the process of sodium diffusion through thin films. Subsequently, in Section 4, the diffusion numerical modeling that lead to the diffusion coefficients and details of the mathematical, numerical, and geometrical schemes for modeling such diffusion processes are described. In Section 5, extracted diffusion coefficients and data analysis are presented. The analysis of the data examines the rate at which the molybdenum is deposited and its relation to the extent of the oxidation. This culminates in analyzing how the diffusion front for the sodium moves with respect to the film growth. To obtain a full picture, the substrate temperature and extent of oxidation are examined. Finally, conclusions are summarized in Section 6.

2. Experimental Details and Film Characterization

Using DC magnetron sputtering with a PVD 75 system (made by Kurt J. Lesker, Pittsburg, CA, USA), Molybdenum thin films were prepared on soda lime glass (SLG) substrates by depositing for 90 min. The substrate to target distance was 15.24 cm (6 inches), and no substrate biasing was used. The depositions utilized a high purity 5.08 cm (2 inches) molybdenum sputtering target with an argon pressure of 1.33 Pa (10 mTorr) at 100 Watts. During this process, a partial pressure of oxygen compared to argon of 1/100 was introduced to facilitate sodium diffusion. Five different substrate temperatures (T_{SS}), and a control sample, were used to determine the effect of substrate temperature on film and diffused species behavior. The control sample was fabricated at room temperature; the other substrate temperatures used were 50 °C, 100 °C, 150 °C, 200 °C, and 250 °C.

X-ray Diffraction (XRD) was performed to determine the crystal structure of the deposited films. XRD measurements were performed using a MiniFlex II Benchtop X-ray Diffractometer (made by Rigaku, Tokyo, Japan). The main goal of XRD processes was to approximate the grain size within the films; this extracted grain size is key to determine the effective sodium diffusion path in the film. To approximate the grain size, the Scherrer's equation was used. Scherrer's equation relates the width of the peak at its half maximum intensity to an average grain size within the film by:

$$L_g = \frac{K\lambda}{\beta \cos(\theta)},$$ (1)

where L_g is the grain size, θ is the Bragg angle, λ is the source X-ray wavelength, β is the full width at half maximum of the relevant peak, and K is the shape factor. While Scherrer's equation for determining grain size can, at times, be a poor predictor due to the relative small grain size within the molybdenum thin films and the distinct growth structure of molybdenum, it proves to be an excellent tool for determining the grain size orthogonal to the substrate. Sputtered molybdenum films grow in a columnar grain structure with a preferred (110) orientation. In Appendix A, XRD spectra patterns for the molybdenum films deposited on SLG at different substrate temperatures for this work are shown. Scherrer's equation explicitly provides the grain size perpendicular to the miller index, meaning that if we assume that molybdenum thin films have a columnar film structure, this grain size can be thought as the average thickness of one of the columnar grains [12]. For this study, the average grain size L_g was estimated using Scherrer's equation and using full width at half maximum extracted from Figure A1 for each sample. The fit to the peak was done using a Split Pseudo Voigt line shape.

The film thicknesses (h) were obtained using scanning electron microscopy (SEM). SEM measurements were performed using a JSM-6060LV system (made by JEOL, Peabody, MA, USA). The average film thickness was determined to be 500 nm, with small variations due to sputtering power and gas flow fluctuations. As far as the average grain boundary size (L_b) is concerned, using transmission electron microscopy, Lin et al. (1987) [13] found it to be around 3 nm. This value was later used by Forest et al. [3] and will be used in this manuscript. Table 1 provides the grain sizes and film thickness for all the Mo thin film samples. It also shows the grain boundary size to grain size ratios, which are in the same range as the porosity values obtained by Bommersbach et al. [8].
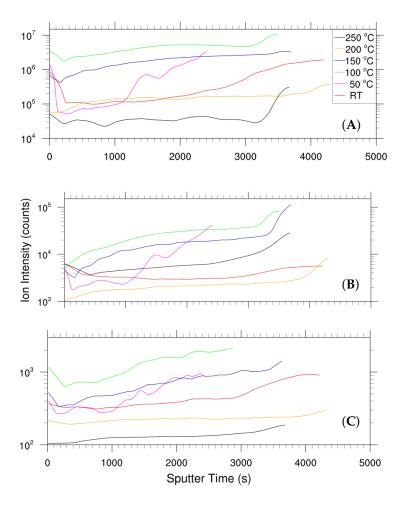
Table 1. Mo film sizes and their grain sizes for various substrate temperatures (a grain boundary size L_b of 3 nm was used).

T_{SS} (°C)	Grain Size (L_g) (nm)	Film Thickness (h) (nm)	$\frac{L_b}{(L_b+L_g)}$
RT	5.0	550	0.375
50	7.8	450	0.278
100	8.5	500	0.261
150	10.4	490	0.224
200	15.0	530	0.167
250	29.7	500	0.092

Dynamic secondary ion mass spectrometry (SIMS) was used to generate the ion profiles of sodium (Na), oxygen (O), and potassium (K) through the Mo thin films. SIMS measurements were performed using a ION TOF TOF-SIMS equipment. Figure 1 presents the SIMS depth profile of Na, O, and K for the films deposited at each substrate temperature. For each atomic species, the highest intensity is found to be at the Mo/SLG interface (right side of each figure). There are several reasons for that: (1) Both sodium and potassium originate from the SLG; (2) when the films are beginning to coalesce into the columnar structure, it is possible for more oxidation to occur because of the higher effective surface area of the molybdenum during the preliminary film coalescence; (3) because the matrix of material is transitioning from an oxidized molybdenum to soda lime glass, it is fairly common to see the intensity of atomic species of small concentration to build-up at such interfaces due to atomic mixing. The sputter time at the peak is related to the film thickness and it can be seen how well it correlates to the film thickness obtained from SEM (Table 1). This paper will focus on analyzing the diffusion process of sodium diffusion only. This is mostly due to the lack of potassium within the substrate. The typical SLG contains 14 wt% Na_2O and only 0.03% K_2O. While we will not be examining the K profiles in detail, similar trends between the Na and K profiles are observed. This implies that both Na and K follow the same diffusion mechanism through the grain boundaries. A local sharp increase of the

intensity is found at the Mo film surface (as sputter time approaches zero). This is the effect of the "accumulation layer" as described by Forest et al. [3].

Figure 1. SIMS depth profiles of (**A**) Sodium, (**B**) Potassium, and (**C**) Oxygen in the molybdenum thin films for different substrate temperatures.

In addition, the resulting oxygen content in the bulk of the molybdenum thin films (after the deposition process) was monitored through the atomic percentages of oxygen detected through X-ray photoelectron spectroscopy (XPS). XPS high resolution measurements were performed using a SPECS system (made by SPECS, Berlin, Germany) with a PHOIBOS 150 Analyzer (made by SPECS, Berlin, Germany).

3. Theoretical Mechanistic Modeling Background

3.1. Relation between Species Concentration and SIMS Intensity Data
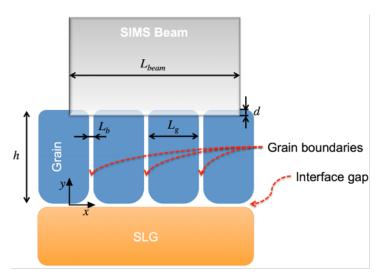
To better understand how to relate a SIMS profile to a diffusion profile, it is helpful to examine the operating principle of dynamic SIMS. During SIMS depth profiling, an ion beam (in this work, cesium ions were used) sputters the sample removing atomic layers from the film. During the sputtering, ions are ejected from the sample and then counted. The profiles presented in the previous section relate the sputtered time within the films to the number of counts per second. The signal intensity level from the output of a SIMS applied to a specimen is related to the presence of an ionic specie. This intensity level (I) is only proportional to the species mass (m) present in a sputtered volume of $V_{beam} = L_{beam}^2 * d$ by SIMS. As shown in Figure 2, d is the depth the SIMS beam sputtered at a fixed δt and L_{beam} is its width (beam cross sectional area is assumed to be a square).

It can be proved that the secondary ion intensity level $I(y)$ is proportional to the average species concentration $\bar{C}(y)$ at any location y and follows (see Appendix B.1):

$$\frac{\bar{C}(y)}{\bar{C}_o} = \frac{I(y)}{I_o},$$

(2)

where C_o and I_o are the average species concentration and the SIMS intensity level, respectively, both at $y = 0$.

Figure 2. Schematic of SIMS beam sputtering molybdenum grains and grain boundaries on a SLG substrate. © (2017) IEEE. Reprinted, with permission, from 2017 IEEE 44th PVSC Proceedings [14].
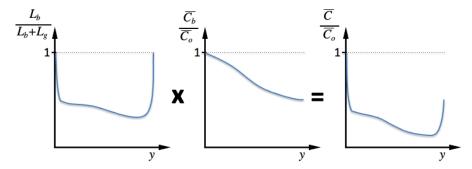
3.2. Relation between Average Species Concentration from SIMS and Average Species Concentration in the Grain and Grain Boundary

It can be observed from Figure 2 that the SIMS intensity level actually provides the species average concentration over multiple grains. Therefore, this overall concentration contains the species concentration information in both the grain and the grain boundary. When the species prefer to diffuse in Mo thin films through the grain boundaries, as it has been reported [3], it can be proved that the species average concentration over multiple grains follows this correlation (see Appendix B.2):

$$\bar{C}(y) = \frac{L_b}{(L_b + L_g)}\bar{C}_b(y).$$

(3)

Therefore, knowing the relationship between $I(y)$ and $\bar{C}(y)$ (Equation (2)), any analysis of the average concentrations provided directly by the SIMS intensity readings could be misled because the average species concentration they show are influenced by the effect of the grain boundary size to grain size ratio. This has not been recognized before. The implication of this is that the SIMS data could provide a profile that could mislead to believe there was a diffusion through grain and grain boundary (Type B diffusion following Harrison [15], as illustrated in the last schematic graph in Figure 3), when in fact all there is a typical concentration profile along the boundaries (Type C diffusion following Harrison [15], as illustrated in the middle schematic graph in Figure 3).
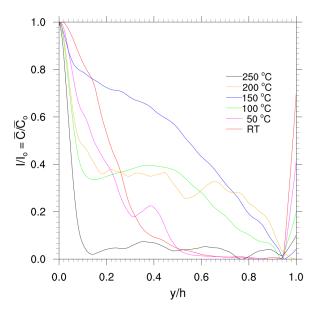
Figure 3. Schematic of the overall average concentration (what the SIMS data provides), which is the product of the grain boundary size to total size ratio and a typical concentration distribution along a straight grain boundary. © (2017) IEEE. Reprinted, with permission, from 2017 IEEE 44th PVSC Proceedings [14].

It is important to point out that the grain boundary size to grain size ratio becomes unity at both, the interface between the thin film and the substrate (at $y = 0$), and at the opposite end (at $y = h$) (also known as the accumulation layer [3]). This is because at both the interface gap and the accumulation layer there is no grain ($L_g = 0$) making the grain boundary size to grain size ratio equal to one regardless of L_b. At the end, the diffusion processes in the interface gap and the accumulation layer behave similarly to one in the grain boundaries.

Figure 4 shows the normalized SIMS profiles for sodium following $\frac{\bar{C}(y)}{\bar{C}_o} = \frac{I(y)}{I_o}$. I_o is the intensity at the interface gap between Mo and SLG. These profiles exhibit the effect of both the average concentration of sodium found in the grain boundaries and the grain boundary size to grain size ratio (following Equation (3)) and are similar to the last schematic graph shown in Figure 3.

Figure 4. Normalized SIMS profiles of sodium in the molybdenum thin films for different substrate temperatures. $y/h = 0$ is the Mo/SLG interface location, and $y/h = 1$ is the accumulation layer location.

3.3. Modeling of the Average Species Concentration in Grain Boundary

For $\bar{C}_b(y)$, a simple one-dimensional mathematical model can be used. As shown in Appendix B.3, the models depend on the boundary conditions. While it is typically assumed that the specie concentration is constant at the base of the thin film ($y/h = 0$), if

the gradient of the specie concentration is zero at the other end of the thin film ($y/h = 1$), the species concentration profile follows [16]:

$$\frac{\bar{C}_b(y,t)}{\bar{C}_o} = 1.0 - 1.2733 \times \cos\left(1.5708\frac{y}{h}\right)e^{-2.4674\frac{Dt}{h^2}}. \tag{4}$$

On the other hand, if the thin film thickness is assumed to be relatively large ($h \sim \infty$) compared to where the diffusion front is at the final time, the species concentration profile follows [17]:

$$\frac{\bar{C}_b(y,t)}{\bar{C}_o} = \text{erfc}\left(\frac{y}{2\sqrt{Dt}}\right). \tag{5}$$

Note that, for both Equations (4) and (5), it was assumed no species presence at early stages (initial condition); thus, the time variable is present in the equations. In this study, this is the final time of the diffusion process, which is also the total molybdenum film deposition time.

4. Numerical Modeling Background

4.1. Geometric Model

Following the previous discussion on the importance of the grain boundary size relative to the grain size, for the numerical model, a geometry consonant with the diffusion path of the alkali ion species is required for the numerical model. As discussed, most of the diffusion occurs through grain boundaries; thus, the model geometry is integral to actively representing the diffusion phenomena. Figure 5A shows a schematic of a typical molybdenum thin film morphology where the dark lines are the grain boundaries. To extract the precise grain boundary geometry (for example, electron microscope images) is not a simple task. In order to create a computationally feasible geometry to simulate diffusion through molybdenum grain boundaries, we relied on five assumptions and observations.
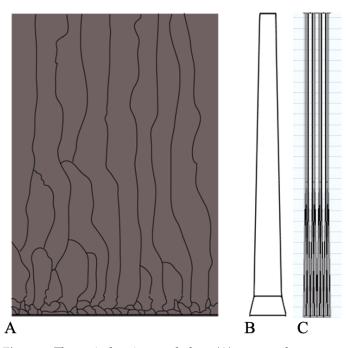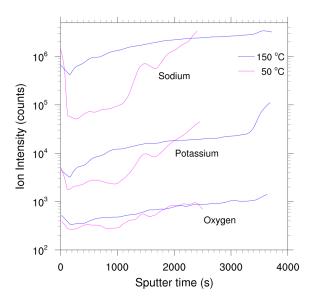

Figure 5. Theoretical grain morphology (**A**) compared to two geometrical models (**B**,**C**).

First, the grain boundary thickness is constant throughout the whole thin film; it was assumed to be 3 nm, following References [3,13]. Second, molybdenum thin films are both columnar and perpendicular to the substrate, and they have only one preferred orientation, along (110). Therefore, little lateral diffusion through the film should occur, which makes the diffusion path mostly one-dimensional. Due to this assumption, it is possible to further

reduce the dimensionality of the system from a 3-dimensional system down to a simple 2-dimensional system.

Figure 6 shows the SIMS profiles for sodium, potassium, and oxygen for molybdenum thin films deposited at both 50 °C and 150 °C. Regardless of the alkali species, some key features can be observed in the profiles that lead to insight on the grain boundary structure. The third observation/assumption is that the peak location for each of the substrate temperature cases is at the same sputter time (same location). This peak is where the Mo/SLG interface is. We assumed that the thickness of such interface is about 3 nm, and that the sodium diffusion coefficient magnitude is orders of magnitude larger than the diffusion coefficient of sodium along the grain boundaries. Due to the proximity of the interface to the SLG (sodium source) and the large diffusion coefficient, the sodium concentration in such interface is always constant.

Figure 6. SIMS profiles of oxygen, potassium, and sodium for the Mo thin films deposited at 50 °C and 150 °C.

Fourth, the rapid increase in concentration at zero sputter time is due to the accumulation layer [3], which is also assumed to be 3 nm thick and with the same sodium diffusion coefficient as in the Mo/SLG interface. Finally, the fifth observation/assumption is that, near the interface, the molybdenum grains do not display columnar shapes, as it is typically observed and assumed in most of the film. While some small grains formed at the beginning of the film deposition can eventually coalesce into larger grains, many others will not coalesce and remain in the final film [18]. In the SIMS profiles an inflection point can be observed where the profile slope changes. It is very important to note that the inflection point is roughly located at the same location regardless of the alkali ion species (see Figure 6). For the 250 °C case, it is at about 3400 s, and, for the 50 °C case, it is at about 2250 s.

Based on these observations, two different geometries were developed and are shown in Figure 5B,C. For the first, following the one-dimensional diffusion path assumption, all grain boundaries were combined into one large diffusion path within our characteristic length. For the second, all grain boundaries within our characteristic length were left independent from each other, and the region between the concentration peak and inflection points was treated by splitting the grain boundary in two (or three).

4.2. Mathematical and Numerical Model

The diffusion phenomena in the developed grain boundary geometry were modeled using COMSOL Multiphysics, which solves the time dependent Fick's Law:

$$\frac{\partial c_i}{\partial t} + \nabla \cdot (-D_i \nabla c_i) = 0, \tag{6}$$

where c_i is the concentration of species i, and D_i is its corresponding diffusivity. No flux on all the boundaries of the domain (except for the boundary at the Mo/SLG interface) were used as boundary conditions. At the Mo/SLG interface, a constant concentration was fixed. As for the initial conditions, it was assumed that the concentrations were zero. A mesh sensitivity analysis for all the domains was performed in order to ensure minimal numerical error.

To determine the diffusion coefficient, a trial-and-error scheme can be performed where the root-mean-square of the difference of the simulated concentration profiles and the normalized SIMS profiles at several fixed film locations is monitored. The final diffusion coefficient can be determined to be when the root-mean-square of the difference is minimum.

5. Results and Discussion

Computational diffusion modeling was performed for all the molybdenum thin films following the trial-and-error scheme to obtain the corresponding diffusion coefficients. All geometrical models were tried for all substrate temperatures. For the splitting grain boundary cases (Figure 5C), three-way, two-way, and no split modes were tested. Figure 7 shows the RMS error obtained in the trial-and-error scheme for the thin film deposited at room temperature with grain boundary split in two. The minimum error was observed at a diffusion coefficient of 1.85×10^{-14} cm^2/s. Figure 8 shows how close the simulated concentration and the normalized SIMS profiles are.
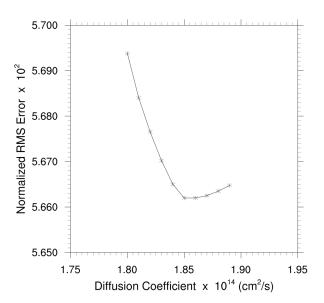

Figure 7. RMS Error for the case of Room Temperature.

For the substrate temperature cases of 100 °C, 150 °C, 200 °C, and 250 °C, it was not possible to get a minimum root-mean-square (RMS) error (see Figure 9). This can only happen if the film is fully saturated with sodium at the end of the deposition. Because either partial or full saturation occurs during the deposition process, it is not possible to discern the diffusivity of sodium through molybdenum grain boundaries with the experimental data. More on this will be discussed later.
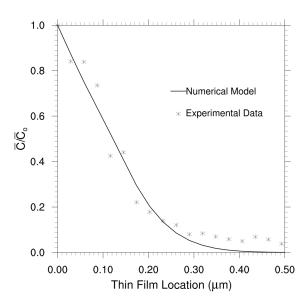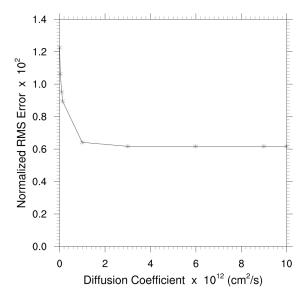
Figure 8. Comparison of the numerical profile and SIMS profile for RT case.

Figure 9. RMS Error for the case of 200 °C.

Table 2 presents all diffusion coefficients for RT and 50 °C cases for different geometrical models. The case of multiple simple grain boundaries with three ways split near interface was not realized for RT because it was not geometrically feasible (the 3 nm grain boundaries would overlap). Analyzing all the values, it can be noted that there is no major effect of the actual geometrical model near the interface on the diffusion coefficients. All diffusion coefficients are reasonable when compare to the ones found in the literature [3]. They reported larger values in the order of 10^{-12} and 10^{-13} cm^2/s, but they are for higher temperatures of 300 to 400 °C. The temperature dependence of a diffusion coefficient typically follows an Arrhenius type relation:

$$D = D_o e^{-\frac{E_a}{RT}}, \tag{7}$$

where E_a is the apparent activation energy for grain boundary diffusion, and D_o is the pre-exponential factor. Diffusion coefficients increase with temperature. One important observation from Table 2 is the diffusion coefficient for 50 °C is counter-intuitively lower than the one for RT. We must consider that there are unavoidable experimental uncertainties

during the film growth, which could lead to a diffusion path different to the one our model predicts; and during SIMS, which could lead to a biased experimental intensity (concentration) profile.

Table 2. Diffusion coefficients (cm^2/s).

Temperature	Collective Boundaries	Multiple Boundaries	Multiple Boundaries: Two Way Split near Interface	Multiple Boundaries: Three Way Split near Interface
RT	2.00×10^{-14}	2.65×10^{-14}	1.85×10^{-14}	—
50 °C	9.00×10^{-15}	1.00×10^{-14}	9.00×10^{-15}	8.00×10^{-15}

Having only two diffusion coefficients at two different temperatures is not enough to get a statistically acceptable activation energy. Some authors have reported values of 117 kJ/mol [3] and 40 kJ/mol [11]. Assuming that the diffusion mechanism in previous work is the same as in this work and that the activation energy does not depend on the oxygen content, we could use those activation energy values. The oxygen content should not affect the activation energy, but it could affect the pre-exponential factor in Arrhenius expression.

With those reported activation energies and our diffusion coefficients at RT and 50 °C, we obtained the pre-exponential factors: 8.27×10^5 cm^2/s using E_a from Reference [3], and 1.87×10^{-8} cm^2/s using E_a from Reference [11]. Figure 10 shows the Arrhenius theoretical curves using both sets of activation energy and pre-exponential factor. The lower activation energy from Reference [11] seems to better predict the diffusion coefficient for a couple of reasons. First, the pre-exponential factor represents the diffusion coefficient at extremely large temperatures. The one using E_a from Reference [3] seems to be extremely large while the other is more reasonable. Second, the diffusion coefficient theoretical prediction is closer to the experimental values when E_a from Reference [11] is used, and third, the predicted diffusion coefficients at the range temperature of 300 °C and 400 °C are in the order of 10^{-11} cm^2/s, which is closer to the values reported in Reference [3]. Our prediction is still larger but the oxygen content is larger in our case. We will, therefore, adopt the activation energy found by Reference [11] for this work.

Figure 10. Arrhenius theoretical curves using two different activation energies.

While diffusion coefficients could not be easily extracted from the higher temperature films due to their pseudo-saturated behavior, the methodology used to form the proposed diffusion profiles still showed consistent results. The dimensional reduction techniques used further facilitate the validity of these techniques for dimensionality reduction of columnar thin films.

5.1. Oxygen Content

As mentioned in the experimental section, oxygen was intentionally and continuously provided in the chamber during deposition; thus, the grain boundaries should be saturated with oxygen. The question is whether the oxygen could also be within the Mo grain. The oxidation of molybdenum has been as subject of various studies. For example, Gulbransen et al. proposed an Arrhenius type of equation for Mo oxidation rate under chemical control (no transport process control) [19]. They proposed the following equation:

$$\frac{dn}{dt} = 3.4305 \times 10^{21} \left[\frac{\text{atoms}}{\text{cm}^2\text{s}}\right] e^{-\frac{19.63\left[\frac{\text{kcal}}{\text{mol}}\right]}{RT}}, \tag{8}$$

where dn/dt is the rate of reaction in [atoms/cm^2/s]. With the use of molybdenum density and molecular weight, and Avogadro number, we can convert this rate of reaction to speed of oxidation (see Table 3). For the range of substrate temperatures in this work, since the speed at which the molybdenum atoms are stacked to form the grain is 1 to 8 orders of magnitude faster than the speed of any molybdenum oxide to form, it is highly unlikely that molybdenum oxide gets formed within the grain. However, molybdenum atoms are still exposed to oxygen at the grain boundaries, where oxidation continues. We, therefore, conclude that the oxygen is not within the molybdenum grain but only at the grain boundaries. Thus, the oxygen SIMS profiles should also follow Equation (3).
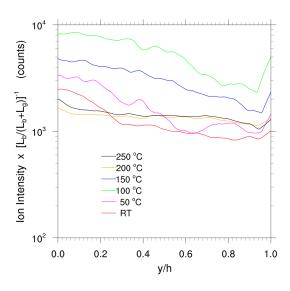
Table 3. Comparison of oxidation speed to film growth.

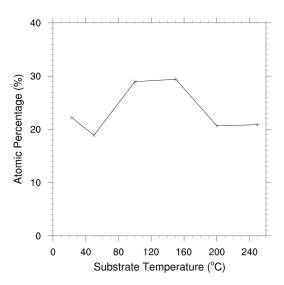| T_{SS} (°C)	dn/dt $\left(\frac{\text{atoms}}{\text{cm}^2\text{s}}\right)$	Oxidation Speed (nm/s)	Film Growth Speed (nm/s)
RT	1.3×10^7	1.8×10^{-9}	0.10
50	1.8×10^8	2.8×10^{-8}	0.08
100	1.1×10^{10}	1.7×10^{-7}	0.09
150	2.5×10^{11}	3.9×10^{-6}	0.09
200	3.0×10^{12}	4.6×10^{-4}	0.10
250	2.2×10^{13}	3.4×10^{-3}	0.09

From Equation (3) and recalling the relation between SIMS intensity and species concentration in Equation (2), to determine the corrected SIMS intensity that shows the oxygen content in the grain boundary only, we divide the intensity values by the respective grain boundary to grain size ratio ($\frac{L_b}{L_b+L_g}$) values from Table 1. The results are shown in Figure 11. In theory, since the oxygen was always present in the chamber, the corrected SIMS intensity should be a relative constant value across the whole film. This did not occur precisely because we do not have the exact $\frac{L_b}{L_b+L_g}$ profile within the film; however, we note that, except for the cases of substrate temperatures of 100 °C and 150 °C, the curves overlap relatively closely. This overlapping of the curves after dividing the intensity by the respective grain boundary to grain size ratio ($\frac{L_b}{L_b+L_g}$) is another evidence of the effect of this ratio on the SIMS profiles.

It is not clear yet why there is an excess of oxygen in the molybdenum films for 100 °C, and 150 °C, but such excess is confirmed with the atomic percentages of oxygen detected through XPS (see Figure 12). As mentioned before, oxygen has effectively been found to facilitate sodium diffusion through Mo and CIGS films. Thus, the oxygen excess in those particular cases could be one of the reasons why the Na SIMS profiles exhibits saturation for the cases of substrate temperatures of 100 °C, and 150 °C. One could expect that the two saturated Na SIMS profiles and the O SIMS profiles in Figure 1A,C would be the same because both species are saturated in the grain boundary; however, they are not. This is an indication that the sodium and oxygen are both in the grain boundary but at different locations within the boundary. The oxygen should be predominantly on the grain surface exposed to the grain boundary, whereas the sodium seems to be located throughout the whole grain boundary.

Figure 11. Normalized SIMS profile for oxygen. The intensity was divided by the grain boundary size to grain size ratio. Most of the curves overlap with each other, following a similar trend. The cases for 100 and 150 °C are off trend.

Figure 12. Atomic percentages of oxygen in the bulk of the film at different substrate temperatures as determined by XPS measurements.

5.2. Film Growth Speed vs. Diffusion Front Speed

In contrast to the previous work on sodium diffusion in molybdenum thin films, in this work, the sodium diffusion occurs while Mo films are deposited on soda lime glass. Thus, the speed of the film growth is important to compare against the diffusion front speed. The film growth speed is simply calculated by

$$S_{\text{film}} = \frac{h}{t}, \tag{9}$$

where h is the film thickness (from Table 1), and t is the total deposition time, which was the same for all the samples: 1.5 h (5400 s). The diffusion front speed is estimated by

$$S_{\text{diff}} = \frac{h_{\text{diff}}}{t}, \tag{10}$$

where h_{diff} is the specie front location after the total deposition time. This can be estimated by $(Dt)^{1/2}$ [20]; thus, the diffusion front speed becomes

$$S_{\text{diff}} = \left(\frac{D}{t}\right)^{1/2}. \tag{11}$$

D can be estimated by using the Arrhenius expression, for which we use the activation energy by Zeller et al. Table 4 shows all those values and the speed ratio, which is the ratio $\frac{S_{\text{diff}}}{S_{\text{film}}}$.

Table 4. Comparison of film growth and diffusion front speed.

T (°C)	Thickness (nm)	Growth Speed (nm/s)	D (cm²/s)	Front Speed (nm/s)	Speed Ratio
RT	550	0.102	8.42×10^{-15}	0.013	0.12
50	450	0.083	2.86×10^{-14}	0.023	0.28
100	500	0.093	1.72×10^{-13}	0.056	0.61
150	490	0.091	6.76×10^{-13}	0.112	1.23
200	530	0.098	1.99×10^{-12}	0.192	1.96
250	500	0.093	4.78×10^{-12}	0.297	3.21

From Table 4, one can observe that, for the cases of 150 °C, 200 °C, and 250 °C, the diffusion front moves faster than the film growth; thus, the film will be saturated with sodium at the end of deposition. This explains the saturated SIMS profiles for those cases. On the other hand, for the cases of RT, 50 °C, and 100 °C, the film growth is faster.

5.3. Substrate Temperature Effect

Examining Equation (3), it can be deduced that the overall concentration of sodium in the thin film depends on two factors: (1) the grain boundary size to grain size ratio $\left(\frac{L_b}{L_b + L_g}\right)$, and (2) the actual concentration of sodium in the grain boundary ($\bar{C}_b$). The grain boundary size to grain size ratio decreases with increasing substrate temperature (larger grains, less boundaries in a fixed space). The specie concentration depends on the diffusion coefficient, which increases with substrate temperature (Arrhenius equation behavior). Since each factor depends differently on temperature, when one increases, the other one decreases. At large temperatures, the grains are larger reducing the number of paths through which the sodium could diffuse, while at low temperatures, the diffusion coefficient is not large enough to allow the sodium to diffuse. This implies that there should be a temperature at which the concentration of sodium is the highest.

To study this in more details, one can look at Table 1 for the overall grain boundary size to grain size ratio. As for the overall concentration of sodium in the grain boundary, we do not have enough information from the experiments to evaluate it because the SIMS profiles show evidence of sodium saturation in most of the samples. Thus, the simple one-dimensional mathematical models, shown in Section 3.3, can be used. Those expressions provide a concentration at any given film location. To get an overall concentration of sodium in the grain boundary, one can take the average across the film:

$$\bar{\bar{C}}_b = \frac{\int_0^h \bar{C}_b(y)dy}{h}, \tag{12}$$

which leads to

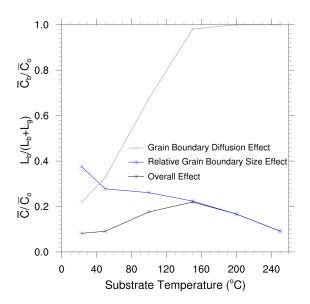$$\frac{\bar{\bar{C}}_b}{\bar{C}_o} = 1.0 - 1.2733 \times \frac{\sin(1.5708)}{1.5708} e^{-2.4674 \frac{Dt}{h^2}} \tag{13}$$

for the case of Equation (4), and

$$\frac{\bar{\bar{C}}_b}{\bar{C}_o} = \text{erfc}\left(\frac{h}{2\sqrt{Dt}}\right) + \frac{2}{h}\sqrt{\frac{Dt}{\pi}}\left(1 - e^{\frac{h^2}{4Dt}}\right) \tag{14}$$

for the case of Equation (5).

Figure 13 shows $\frac{\bar{\bar{C}}_b}{\bar{C}_o}$ using Equation (13) for the different substrate temperatures (light gray curve—grain boundary diffusion effect). Note that the model predicts overall saturation of sodium ($\frac{\bar{\bar{C}}_b}{\bar{C}_o} \sim 1$) for substrate temperatures larger than 150 °C. The values of the relative grain boundary size $\frac{L_b}{L_b+L_g}$ from Table 1 are also shown (blue curve—relative grain boundary size effect). Following Equation (3), both of these factors were multiplied to obtain the overall concentration of sodium in the bulk of the thin film (black curve—overall effect). As discussed above, our model predict that a maximum concentration of sodium should be detected by SIMS in the temperature range of 100 °C to 200 °C. Similar findings were observed using Equation (14) for the grain boundary diffusion effect (results not shown). This finding is yet another evidence of why the SIMS profiles for such temperatures show saturation. The simple mathematical models also show that the grain boundaries could be saturated for high substrate temperatures, as it was observed in the corresponding SIMS profiles.

Figure 13. Prediction of the overall concentration of sodium in the bulk of the Mo thin films, assuming the sodium concentration profile in the grain boundary follows an exponential function only.

6. Conclusions

In this paper, we analyzed the sodium diffusion behavior in oxidized molybdenum thin films deposited on soda-lime glass at different substrate temperatures. Several observations were made after the analysis. First, we demonstrated that it is extremely important to consider the grain boundary size to grain size ratio when studying species diffusion in solid thin films. Second, substrate temperature has been thought as a key parameter in the diffusion of alkali ions through the molybdenum thin films due to its well-known effect in the diffusion coefficient. However, it also affects the grain boundary size to grain size ratio by decreasing it. This behavior implies that there is a range of temperatures where a maximum overall specie concentration can be found in a solid thin film. Third, as others have observed, the presence of oxygen notably affects the effective diffusion of sodium in molybdenum thin films. The oxygen is likely located at the grain boundaries. Fourth, the speed at which the molybdenum is deposited on the soda-lime glass also plays an important role in the diffusion of sodium. If the film growth is slow, the sodium could reach

saturation in the grain boundaries quickly. And, finally, a diffusion modeling via COMSOL, with an appropriate grain boundary to grain geometry, can allow the determination of species diffusion coefficients that match dynamic SIMS profiles.

Author Contributions: Conceptualization, O.A.; methodology, B.B., J.A., and O.A.; validation, T.A., G.R., S.K., and D.P.; formal analysis, O.A. and B.B.; investigation, T.A., G.R., S.K., D.P., B.B.; resources, S.M.; data curation, B.B.; writing—original draft preparation, O.A.; writing—review and editing, B.B. and S.M.; visualization, B.B. and O.A.; supervision, S.M.; project administration, S.M.; funding acquisition, S.M. All authors have read and agreed to the published version of the manuscript.

Institutional Review Board Statement: Not applicable.

Informed Consent Statement: Not applicable.

Data Availability Statement: The data presented in this study are available on request from the corresponding author.

Conflicts of Interest: The authors declare no conflict of interest.

Abbreviations

The following abbreviations are used in this manuscript:

CIGS	$Cu(In,Ga)Se_2$
K	Potassium
Mo	Molybdenum
Na	Sodium
O	Oxygen
RMS	Root mean square
RT	Room temperature
SEM	Scanning electron microscopy
SLG	Soda lime glass
SIMS	Secondary ion mass spectrometry
XPS	X-ray photoelectron spectroscopy
XRD	X-ray diffraction

Symbols

The following symbols are used in this manuscript:

$\bar{C}(y)$	Average species concentration
$\bar{C}_b(y)$	Average species concentration in grain boundary
$\bar{\bar{C}}_b$	Average species concentration in grain boundary across the film
$\bar{C}_o$	Average species concentration at the Mo/SLG interface
D	Diffusion coefficient
D_o	Arrhenius pre-exponential factor
d	SIMS sputtered depth
E_a	Arrhenius apparent activation energy
h	Thin film thickness
h_{diff}	Specie front location
$I(y)$	Secondary ion intensity level
I_o	Secondary ion intensity level at the Mo/SLG interface
L_b	Average grain boundary size
L_{beam}	SIMS beam width
L_g	Average grain size
n	Number of atoms
R	Universal gas constant

S_{film}	Film thickness growth speed
S_{diff}	Diffusion front speed
t	time
T_{SS}	Substrate temperature
V_{beam}	SIMS sputtered volume
y	Any location in the thin film

Appendix A. XRD Spectra of Molybdenum Films

Figure A1. Broad XRD spectra of the sputtered molybdenum films (**left**) and the (110) peak (**right**) with varying substrate temperatures.

Appendix B. Theoretical Model

Appendix B.1. Relation between Species Concentration and SIMS Intensity Data

Following the work by Ayala et al. [14], the intensity level (*I*) SIMS detects is only proportional to the species mass (*m*) present in a sputtered volume of $V_{beam} = L_{beam}^2 * d$. As shown in Figure 2, *d* is the depth the SIMS beam sputtered at a fixed δt, and L_{beam} is its width (beam cross sectional area is assumed to be a square). In addition, as it can observed in Figure 2, the grains and grain boundaries size (L_g and L_b, respectively) are related to L_{beam} as follows: $L_{beam} = N_g(L_b + L_g)$. N_g is the number of grains the SIMS beam is sputtering (assuming a uniform average grain size, as seen by SEM).

The secondary ion intensity level is correlated to the average species concentration, $\bar{C}(y)$, in the sputtered volume from the definition of average concentration as follows:

$$\bar{C}(y) = \frac{\int_0^{L_{beam}} C(x,y)dx}{L_{beam}} = \frac{\int_0^{N_g(L_b+L_g)} C(x,y)dx}{N_g(L_b+L_g)}$$
$$= \frac{N_g\left[\int_0^{L_b} C_b(x,y)dx + \int_{L_b}^{L_b+L_g} C_g(x,y)dx\right]}{N_g(L_b+L_g)}, \tag{A1}$$

where $C_b(x,y)$ is the specie concentration in the grain boundary, and $C_g(x,y)$ is the specie concentration in the grain. Assuming no variations in the direction perpendicular to Figure 2, specie concentration is related to specie mass as $dm_g = C_g(x,y) * d * L_{beam} * dx$ for the mass in the grain and $dm_b = C_b(x,y) * d * L_{beam} * dx$ for the mass in the grain boundary. Introducing both in the above equation, it becomes:

$$\bar{C}(y) = \frac{N_g\left[\int_0^{L_b} dm_b + \int_{L_b}^{L_b+L_g} dm_g\right]}{d * L_{beam} * N_g(L_b+L_g)}. \tag{A2}$$

The numerator is directly proportional to the intensity level (I); thus, $\bar{C}(y)$ is directly proportional to I (i.e., $\bar{C}(y) \propto I(y)$). Therefore, normalizing $\bar{C}(y)$ with the concentration at $y = 0$ (C_o) yields:

$$\frac{\bar{C}(y)}{\bar{C}_o} = \frac{I(y)}{I_o}. \tag{A3}$$

Appendix B.2. Relation between Average Species Concentration from SIMS and Average Species Concentration in the Grain and Grain Boundary

It can be observed from Figure 2 that the SIMS intensity level actually provides the species average concentration over multiple grains. Therefore, this overall concentration contains the species concentration information in both the grain and the grain boundary [14]. Therefore, considering the average species concentration in the grain ($\bar{C}_g(y)$) and in the grain boundary ($\bar{C}_b(y)$) in Equation (A1), we obtain the overall average species concentration in the film:

$$\bar{C}(y) = \frac{L_g}{(L_b + L_g)} \bar{C}_g(y) + \frac{L_b}{(L_b + L_g)} \bar{C}_b(y). \tag{A4}$$

Many authors have stated that most of the species diffusion in Mo thin films occurs through the grain boundaries [3]. Assuming that is the case, Equation (A4) can be simplified to:

$$\bar{C}(y) = \frac{L_b}{(L_b + L_g)} \bar{C}_b(y). \tag{A5}$$

Therefore, the overall average concentration depends on both the local average concentration found in the grain boundaries and the grain boundary size to grain size ratio.

Appendix B.3. Modeling of the Average Species Concentration in Grain Boundary

For $\bar{C}_b(y)$, we propose a simple one-dimensional mathematical model. Most diffusion mathematical models depend on the initial and the boundary conditions. The initial condition of preference is:

$$\bar{C}_b(y, t = 0) = 0. \tag{A6}$$

Choosing the boundary conditions of

$$\bar{C}_b(y = 0, t) = \bar{C}_o, \text{ and } \frac{\partial \bar{C}_b(y = h, t)}{\partial y} = 0, \tag{A7}$$

the solution of the Fick's law differential equation can be obtained following Bergman et al. [21]:

$$\frac{\bar{C}_o - \bar{C}_b(y, t)}{\bar{C}_o} = \sum_{n=1}^{\infty} K_n \times \cos\left(\lambda_n \frac{y}{h}\right) e^{-\lambda_n^2 \frac{Dt}{h^2}}, \tag{A8}$$

where K_n is defined as

$$K_n = \frac{\sin \lambda_n}{2\lambda_n + \sin 2\lambda_n}. \tag{A9}$$

The values of λ_n are obtained from the transcended equation

$$\lambda_n + \tan \lambda_n = A, \tag{A10}$$

where λ_n represents the eigenvalues, and A is a very large number. Incropera et al. [16] have found that, for certain conditions (such as a diffusion processes occurring during a

long time), the series solution can be approximated with only the leading term; thus, the equation becomes after short manipulations:

$$\frac{\bar{C}_b(y,t)}{\bar{C}_o} = 1.0 - 1.2733 \times \cos\left(1.5708\frac{y}{h}\right)e^{-2.4674\frac{Dt}{h^2}}. \tag{A11}$$

Another simple one-dimensional mathematical model, assuming the following boundary conditions

$$\bar{C}_b(y = 0, t) = \bar{C}_o, \text{ and } \frac{\partial \bar{C}_b(y = \infty, t)}{\partial y} = 0, \tag{A12}$$

is found in Sze et al. [17] as:

$$\frac{\bar{C}_b(y,t)}{\bar{C}_o} = \text{erfc}\left(\frac{y}{2\sqrt{Dt}}\right). \tag{A13}$$

References

1. Rudmann, D.; da Cunha, A.F.; Kaelin, M.; Kurdesau, F.; Zogg, H.; Tiwari, A.N.; Bilger, G. Efficiency Enhancement of Cu(In,Ga)Se$_2$ Solar Cells due to Post-deposition Na Incorporation. *Appl. Phys. Lett.* **2004**, *84*, 1129–1131. [CrossRef]
2. Chirila, A.; Reinhard, P.; Pianezzi, F.; Bloesch, P.; Uhl, A.; Fella, C.; Kranz, L.; Keller, D.; Gretener, C.; Hagendorfer, H.; et al. Potassium-induced Surface Modification of Cu(In,Ga)Se$_2$ Thin Films for High-efficiency Solar Cells. *Nat. Mater.* **2013**, *12*, 1107–1111. [CrossRef] [PubMed]
3. Forest, R.; Eser, E.; McCandless, B.E.; Birkmire, R.W. Understanding the Role of Oxygen in the Segregation of Sodium at the Surface of Molybdenum Coated Soda-Lime Glass. *AIChE J.* **2014**, *60*, 2365–2372. [CrossRef]
4. Bodegard, M.; Granath, K.; Stolt, L.; Rockett, A. The behaviour of Na Implanted into Mo Thin Films During Annealing. *Sol. Energy Mater. Sol. Cells* **1999**, *58*, 199–208. [CrossRef]
5. Granath, K.; Stolt, L.; Bodegard, M.; Rockett, A.; Schroeder, D.L. Sodium in Sputtered Mo Back Contacts for Cu(In,Ga)Se$_2$ Devices: Incorporation, Diffusion, and Relationship to Oxygen. In Proceedings of the 14th European Photovoltaic Solar Energy Conference, Barcelona, Spain, 30 June–4 July 1997; pp. 1278–1282.
6. Yoon, J.H.; Seong, T.Y.; Jeong, J.H. Effect of a Mo Back Contact on Na Diffusion in CIGS Thin Film Solar Cells. *Prog. Photovolt. Res. Appl.* **2013**, *21*, 58–63. [CrossRef]
7. Assmann, L.; Bernede, J.C.; Drici, A.; Amory, C.; Halgand, E.; Morsli, M. Study of the Mo Thin Films and Mo/CIGS Interface Properties. *Appl. Surf. Sci.* **2005**, *246*, 159–166. [CrossRef]
8. Bommersbach, P.; Arzel, L.; Tomassini, M.; Gautron, E.; Leyder, C.; Urien, M.; Dupuy, D.; Barreau, N. Influence of Mo Back Contact Porosity on Co-Evaporated Cu(In,Ga)Se$_2$ Thin Film Properties and Related Solar Cell. *Prog. Photovolt. Res. Appl.* **2013**, *21*, 332–343. [CrossRef]
9. Eser, E.; Fields, S.; Hanket, G.; Birkmire, R.W.; Doody, J. Critical Issues in Vapor Deposition of Cu(InGa)Se$_2$ on Polymer Web: Source Spitting and Back Contact Cracking. In Proceedings of the 31st IEEE Photovoltaic Specialists Conference, Lake Buena Vista, FL, USA, 3–7 January 2005; pp. 515–518.
10. Akcay, N.; Akin Sonmez, N.; Zaretskaya, E.P.; Ozcelik, S. Influence of deposition pressure and power on characteristics of RF-Sputtered Mo films and investigation of sodium diffusion in the films. *Curr. Appl. Phys.* **2018**, *18*, 491–499. [CrossRef]
11. Zellner, M.B.; Birkmire, R.W.; Eser, E.; Shafarman, W.N.; Chen, J.G. Determination of Activation Barriers for the Diffusion of Sodium through CIGS Thin-Film Solar Cells. *Prog. Photovolt. Res. Appl.* **2003**, *11*, 543–548. [CrossRef]
12. Vorokh, A.S. Scherrer formula: Estimation of Error in Determining Small Nanoparticle Size. *Nanosyst. Phys. Chem. Math.* **2018**, *9*, 364–369. [CrossRef]
13. Lin, J.S.; Budhani, R.C.; Bunshah, R.F. Effects of Substrate Bias on the Resistivity and Microstructure of Molybdenum and Molybdenum Silicide Films. *Thin Solid Films* **1987**, *153*, 359–368. [CrossRef]
14. Ayala, O.; Akwari, C.; Ashrafee, T.; Karki, S.; Rajan, G.; Marsillac, S. Grain and Grain Boundary Geometrical Shape Considerations on Sodium and Potassium Diffusion Through Molybdenum Films. In Proceedings of the 2017 IEEE 44th Photovoltaic Specialist Conference (PVSC), Washington, DC, USA, 25–30 June 2017; pp. 735–737.
15. Harrison, L.G. Influence of Dislocations on Diffusion Kinetics in Solids with Particular Reference to the Alkali Halides. *Trans. Faraday Soc.* **1961**, *57*, 1191–1199. [CrossRef]
16. Incropera, F.P.; DeWitt, D.P.; Bergman, T.L.; Lavine, A.S. *Fundamentals of Heat and Mass Transfer*, 6th ed.; John Wiley & Sons Inc.: Hoboken, NJ, USA, 2007.
17. Sze, S.M.; Lee, K.M. *Semiconductor Devices—Physics and Technology*, 3rd ed.; John Wiley & Sons Inc.: Hoboken, NJ, USA, 2012.
18. Petrov, I.; Barna, P.B.; Hultman, L.; Greene, J.E. Microstructural Evolution During Film Growth. *J. Vac. Sci. Technol. A* **2003**, *21*, S117–S128. [CrossRef]

19. Gulbransen, E.A.; Andrew, K.F.; Brassart, F.A. Oxidation of Molybdenum 500 °C to 1700 °C. *J. Electrochem. Soc.* **1963**, *110*, 952–959. [CrossRef]
20. Kaur, I.; Mishin, Y.; Gust, W. *Fundamentals of Grain and Interphase Boundary Diffusion*, 3rd ed.; John Wiley & Sons Inc.: Hoboken, NJ, USA, 1995.
21. Bergman, T.L.; Lavine, A.S.; Incropera, F.P.; DeWitt, D.P. *Introduction to Heat Transfer*, 6th ed.; John Wiley & Sons Inc.: Hoboken, NJ, USA, 2011.